Draft version April 18, 2018
Typeset using LaTeX **modern** style in AASTeX62

NICER Discovers the Ultracompact Orbit of the Accreting Millisecond Pulsar IGR J17062−6143

T. E. Strohmayer,[1] Z. Arzoumanian,[2] S. Bogdanov,[3] P. M. Bult,[4] D. Chakrabarty,[5] T. Enoto,[6] K. C. Gendreau,[2] S. Guillot,[7,8] A. K. Harding,[1] W. C. G. Ho,[9,10] J. Homan,[11,12] G. K. Jaisawal,[13] L. Keek,[14] M. Kerr,[15] S. Mahmoodifar,[1] C. B. Markwardt,[2] S. M. Ransom,[16] P. S. Ray,[15] R. Remillard,[5] and M. T. Wolff[15]

[1] *Astrophysics Science Division and Joint Space-Science Institute, NASA's Goddard Space Flight Center, Greenbelt, MD 20771, USA*
[2] *X-ray Astrophysics Laboratory, Astrophysics Science Division, NASA's Goddard Space Flight Center, Greenbelt, MD 20771, USA*
[3] *Columbia Astrophysics Laboratory, Columbia University, 550 West 120th Street, New York, NY 10027, USA*
[4] *Astrophysics Science Division, NASA's Goddard Space Flight Center, Greenbelt, MD 20771, USA*
[5] *MIT Kavli Institute for Astrophysics and Space Research, Massachusetts Institute of Technology, Cambridge, MA 02139, USA*
[6] *The Hakubi Center for Advanced Research and Department of Astronomy, Kyoto University, Kyoto 606-8302, Japan*
[7] *CNRS, IRAP, 9 avenue du Colonel Roche, BP 44346, F-31028 Toulouse Cedex 4, France*
[8] *Universit de Toulouse, CNES, UPS-OMP, F-31028 Toulouse, France*
[9] *Department of Physics and Astronomy, Haverford College, 370 Lancaster Ave., Haverford, PA 19041, USA*
[10] *Mathematical Sciences, Physics and Astronomy, and STAG Research Centre, University of Southampton, Southampton SO17 1BJ, United Kingdom*
[11] *Eureka Scientific, Inc., 2452 Delmer Street, Oakland, CA 94602, USA*
[12] *SRON, Netherlands Institute for Space Research, Sorbonnelaan 2, 3584 CA Utrecht, The Netherlands*
[13] *National Space Institute, Technical University of Denmark, Elektrovej 327-328, DK-2800, Lyngby, Denmark*
[14] *Department of Astronomy, University of Maryland College Park, MD 20742, USA*
[15] *Space Science Division, Naval Research Laboratory, Washington, DC 20375-5352, USA*
[16] *National Radio Astronomy Observatory, Charlottesville, VA 22903, USA*

ABSTRACT

We present results of recent *Neutron Star Interior Composition Explorer* observations of the accreting millisecond X-ray pulsar IGR J17062−6143 that show that it resides in a circular, ultracompact binary with a 38 minute orbital period. *NICER* observed the source for ≈ 26 ksec over a 5.3 day span in 2017 August, and again for 14 and 11 ksec in 2017 October and November, respectively. A power spectral analysis of the August exposure confirms the previous detection of pulsations at 163.656 Hz in *Rossi X-ray Timing Explorer* data, and reveals phase modulation due to orbital motion of the neutron star. A coherent search for the orbital solution using the Z^2 method finds a best-fitting circular orbit with a period of 2278.21 s (37.97 min), a projected semi-major axis of 0.00390 lt-sec, and a barycentric pulsar frequency of

163.6561105 Hz. This is currently the shortest known orbital period for an AMXP. The mass function is 9.12×10^{-8} $M_\odot$, presently the smallest known for a stellar binary. The minimum donor mass ranges from $\approx 0.005 - 0.007$ $M_\odot$, for a neutron star mass from 1.2 - 2 $M_\odot$. Assuming mass transfer is driven by gravitational radiation, we find donor mass and binary inclination bounds of $0.0175 - 0.0155 M_\odot$ and $19^\circ < i < 27.5^\circ$, where the lower and upper bounds correspond to 1.4 and 2 $M_\odot$ neutron stars, respectively. Folding the data accounting for the orbital modulation reveals a sinusoidal profile with fractional amplitude $2.04 \pm 0.11\%$ (0.3 - 3.2 keV).

Keywords: stars: neutron — stars: oscillations — stars: rotation — X-rays: binaries — X-rays: individual (IGR J17062−6143) — methods: data analysis

1. INTRODUCTION

The accreting neutron star binary IGR J17062−6143 (hereafter, J1706) is one of the most recently identified accreting millisecond X-ray pulsars (AMXP). First observed in outburst in 2006 (Churazov et al. 2007; Ricci et al. 2008; Remillard & Levine 2008), it has since then been persistently accreting at luminosities in the range 5.8 - 7.5×10^{35} erg s^{-1} (2 - 20 keV), assuming a distance of 7.3 kpc (Degenaar et al. 2013; Keek et al. 2017; Strohmayer & Keek 2017; van den Eijnden et al. 2018). The object's neutron star nature was first revealed by the detection of thermonuclear X-ray bursts. The first of these was observed by *Swift* in 2012 (Degenaar et al. 2013), and most recently Keek et al. (2017) reported on *Swift* observations of a long duration burst first detected with *MAXI* (Negoro et al. 2015) that was likely powered by burning of a deep helium layer. The properties of these long duration (tens of minutes) thermonuclear X-ray bursts are consistent with the accumulation of helium rich material on the neutron star surface, which could be accommodated by accretion from a degenerate helium dwarf in an ultracompact system. However, accretion of hydrogen-rich fuel under certain conditions can also lead to thick, combustible helium layers, so the observation of apparently helium-powered nuclear flashes is not necessarily a definitive indication of an ultracompact system (Fujimoto et al. 1981; Galloway & Cumming 2006). Strohmayer & Keek (2017), hereafter SK17, reported the detection (4.3σ) of 163.656 Hz pulsations in a single $\approx$ 1200 s observation with the *Rossi X-ray Timing Explorer* (*RXTE*; Bradt et al. (1993)). They found a fractional pulsed amplitude (after background subtraction) of $9.4 \pm 1.1\%$, but could not determine the orbital period of the system due to the single, short *RXTE* observation. They were able to place a lower limit on the orbital period of about 17 minutes.

The source has recently been studied extensively with *Swift*, *NuSTAR*, *Chandra* and *XMM-Newton*. For example, Degenaar et al. (2017) reported the presence of Fe Kα reflection features in *NuSTAR* data, modeling of which suggested an inner disk that may be truncated out to $\approx 100 R_g$, where $R_g = GM/c^2$. Most recently, van den Eijnden et al. (2018) presents results of simultaneous *NuSTAR* and *XMM-*

Newton observations. They report the presence of reflection features as well, and suggest a similarly truncated disk as in Degenaar et al. (2017). They note, however, that a disk extending down to the neutron star cannot be excluded if the binary inclination is very low. Based on analysis of *XMM-Newton* Reflection Grating Spectrometer (RGS) data they also suggest the system may have an oxygen-rich circumbinary environment, perhaps due to an outflow. Interestingly, they also searched for pulsations using the *XMM-Newton* EPIC timing mode data but did not detect them. They placed an upper limit on the pulsed fraction in those data of 5.4% ($0.5-10$ keV). They concluded that the persistently faint X-ray luminosity could be indicative of either an ultracompact binary system or perhaps magnetic truncation, but the spectroscopic data alone were not decisive between these two possibilities. Hernandez Santisteban et al. (2018) have recently reported on broad-band optical to near-infrared (NIR) photometry of J1706 that they modeled as emission from an irradiated accretion disk. Their modeling indicates an accretion disk size consistent with an ultracompact orbit, and they argued for an orbital period in the range from 0.4 - 1 hr. Additionally, their optical spectroscopy showed no H-α emission, consistent with a hydrogen-deficient donor and an ultracompact system. Thus, sensitive, new timing observations to determine the binary orbital parameters, and the nature of the system, were clearly warranted.

In this paper we report results of recent *Neutron Star Interior Composition Explorer* (NICER) observations of J1706. The principal goals of the *NICER* observing campaign were to confirm (or not) the *RXTE* detection of 163.656 Hz pulsations and, if pulsations could be detected, to determine the system's orbital parameters. We show below that the new *NICER* data confirm that J1706 is an 163.656 Hz pulsar, and also reveal an ultracompact orbit with similarities to other ultracompact AMXPs (Patruno & Watts 2012). The plan of the paper is as follows. We first describe the observations, data selection, and our initial pulsation search and detection, confirming that J1706 is a 163.656 Hz pulsar. We next discuss our orbit search and detection, and we summarize the properties of the system given the orbit solution. We conclude with a brief summary and discussion of the implications of our findings for the nature of J1706.

2. NICER OBSERVATIONS AND PULSATION SEARCH

NICER was installed on the International Space Station (*ISS*) in 2017 June, and began full science operations after a one month checkout and verification period. *NICER* is optimized for low background, high throughput, fast timing observations across the $0.2-12$ keV band (Gendreau et al. 2012), achieving an absolute timing precision of ≈ 100 ns with the aid of a GPS receiver. We obtained with *NICER* 26 ks of good exposure on J1706 in the time window spanning 2017 August 9 - 15. Additional observations were obtained in October and November, but we focused on the August data for our initial pulsation search. We processed and analyzed the data

using HEASOFT version 6.22 and NICERDAS 2017-09-06_V002. We barycentered the data using the tool *barycorr* employing the *DE200* solar system ephemeris and source coordinates $R.A. = 256.5677°$, decl. $= -61.7113°$ (Ricci et al. 2008). After data processing and selection we identified 58 good time intervals (GTIs) of at least 50 s duration in the August data, for a total of 26 ks of on-source exposure. The on-source dwell times with *NICER* tend to be somewhat shorter than for free-flying, low-Earth orbit observatories. Figure 1 shows the resulting light curve accumulated in 16 s bins, and including events with energies in the range from 0.3 to 5 keV. The average count rate was ≈ 31 s^{-1}, which is consistent with the expected rate estimated using source flux and spectra from recent observations (Degenaar et al. 2017; Keek et al. 2017). We do see evidence for variations in the background counting rates, particularly in the August data. This is most evident in the band above ≈ 5 keV. Based on the average count rate spectrum we estimate that the *NICER* background in the 0.3 to 5 keV band is, on average, less than the source count rate by a factor of ≈ 15. We note that we did not observe any thermonuclear X-ray bursts from the source, but given the long recurrence time, this is not very surprising (Keek et al. 2017).

For our pulsation search we further limited the upper end of the energy band to 3.2 keV due to the higher backgrounds present in some dwells. Our choice here reflected a trade-off between either removing a substantial number of dwells completely or reducing the upper energy threshold somewhat, and thereby allowing us to utilize most of the dwells. To search for pulsations we computed a light curve (0.3 - 3.2 keV) of the full August dataset sampled at 4096 Hz. This light curve spans 500 ksec (≈ 5.8 days) and has $(5 \times 10^5) \times 4096 = 2.048 \times 10^9$ bins. We computed a FFT power spectrum of this light curve and searched in the frequency range in which pulsations were reported by SK17. Figure 2 shows the resulting power spectrum, normalized as in Leahy et al. (1983), in the vicinity of the 163.656 Hz pulse frequency. The red, vertical dashed lines denote the approximate range of pulse frequency detected in the *RXTE* observations. An excess of signal power consistent with this frequency range is clearly evident. The highest power in the plotted frequency range has a value of 56.3. The expected noise power distribution is a χ^2 distribution with 2 degrees of freedom. The probability to exceed this value (56.3) in a single trial is 6×10^{-13}. There are 15,000 frequency bins in the range from 163.64 to 163.67 Hz. This gives a chance occurrence probability of 9×10^{-9} for the highest observed power only. Since additional excess powers are present as well, this is an extremely conservative significance estimate.

In Figure 2 one can see that the pulsar signal is comprised of two main sidebands, each of which is modulated by a number of finely spaced peaks. The first, most significant, sideband is that near the center of the frequency band denoted by the red, vertical lines, and the second is near the high end of the band. There is likely a third sideband mid-way between these two, but it is weak enough that it is harder to discern above the noise. The presence of such sidebands in the power spectrum

is a strong indication of the presence of phase modulation due to orbital motion of the pulsar (Ransom et al. 2003). We do not detect any excess power at higher harmonics of the pulsar frequency. We note that the finely spaced peaks modulating each sideband are consistent with the *ISS* orbit period, thus these result from the incomplete sampling (gaps) in the time series, that is, *NICER*'s window function.

As a further test we also computed power spectra of some of the long individual on-source dwells, and then averaged these. We used 21 of the longest dwells with exposures ranging from 1294 s (longest) to 545 s (shortest). These intervals are indicated in Figure 1 by vertical dashed lines drawn at the center of each interval. For each of these intervals we computed a light curve sampled at 4096 Hz and with a duration of 2048 s. Since this is longer than each of the individual exposures we padded the light curves to 2048 s using the mean value determined from the good exposure in each dwell. This procedure ensures that the same Fourier frequency spacing is used for each interval and facilitates simple averaging of the resulting power spectra. We then computed FFT power spectra for each dwell and averaged them. The resulting power spectrum is shown in Figure 3, and clearly shows an excess of power at the same frequency as is evident in Figure 2. Indeed, we see the same basic signal structure of two dominant sidebands. Thus, *NICER* clearly detects pulsations from J1706 in a frequency range consistent with the earlier *RXTE* detection, and moreover, the sidebands in the power spectra are strongly indicative of accelerated motion of the pulsar.

3. SEARCHING FOR THE ORBIT

Having recovered pulsations from J1706 with *NICER* we next began a search for the orbital parameters. The combination of a weak pulsed signal and relatively short uninterrupted exposures means that it is not really possible to closely track the pulse frequency variations with time around the orbit, particularly if the orbital period is short compared to the typical gap in exposure. It is therefore not possible to directly "see" the orbital frequency evolution with time in, for example, a dynamic power spectrum. This makes it more challenging to deduce the orbit. Nevertheless, orbital motion of the pulsar introduces periodic light travel time delays/advances that depend on its orbital phase. As noted above, these produce a characteristic sideband structure in power spectra computed from a light curve that samples at least several orbital periods (Ransom et al. 2003). In principle, one can measure the orbital period by detecting this sideband structure in the power spectrum, as the frequency spacing of the phase modulation sidebands is set by the orbital period. However, the complex window function (due to the data gaps) associated with *NICER*'s observing windows makes it challenging in the present case to directly infer the orbital period in this way.

Because of the challenges outlined above we employed a coherent, grid search for the orbital parameters using the Z_n^2 statistic (Buccheri et al. 1983;

Strohmayer & Markwardt 2002), and since there is no evidence for harmonic signals we began by restricting the analysis to $n = 1$. The observed population of AMXPs are all in highly circular orbits, and indeed there are good theoretical arguments why this should be the case, so we began our search with circular orbit models. We also start with the assumption that the pulsar frequency does not vary significantly across the August data epoch. We used the Blandford & Teukolsky (1976) relativistic orbit model to parameterize the time delays, and with the assumption of circularity, we have a four parameter search space; the pulsar frequency, ν_0, projected semi-major axis, $a_x \sin i/c$, orbital period, P_{orb}, and the epoch of mean longitude equal to zero, T_0. Mean longitude is the orbit phase angle measured from the ascending node. For a circular orbit, the pulsar is "behind" the companion star at mean longitude of 90°. We evaluate the statistic,

$$Z_1^2 = \left(\sum_{j=1}^{N} \cos\phi_j\right)^2 + \left(\sum_{j=1}^{N} \sin\phi_j\right)^2 , \quad (1)$$

where, $\phi_j = \nu_0(t_j + \Delta t_{BT}(t_j, a_x \sin i/c, P_{orb}, T_0))$, Δt_{BT} is the binary time delay model (Blandford & Teukolsky 1976) as a function of orbital parameters, and t_j are the barycentric photon arrival times. Since such "brute force" searches can be computationally expensive, we began by searching a subset of the full August dataset. For this we used the more densely sampled portion of the light curve, the portion of Figure 1 between about 1.5 and 2.2 days. We set up grids of values spanning the relevant ranges for each parameter. We used the recovered signal in the power spectra (Figures 2 and 3), as well as prior results to guide these choices. For example, SK17 used the *RXTE* data to place a lower limit on the orbital period of about 17 min. As noted above, the sideband structure in the power spectrum is suggestive of a compact orbit. Based on this we confined our initial search to orbital periods between 10 and 90 min. We used the power spectral results to bound both ν_0 and $a_x \sin i/c$. Finally, we employed a sampling in T_0 equivalent to 2° of orbital phase. We then computed Z_1^2 for all combinations of parameters to find candidate solutions with large Z_1^2. This procedure yielded a candidate orbit solution with $Z_1^2 = 77.1$, an orbital period of $P_{orb} = 2278$ s, $a_x \sin i/c = 0.00393$ lt-sec, and $\nu_0 = 163.65611055$ Hz. We did not find any other comparable Z_1^2 maxima within the range of parameter space searched.

Since this result was obtained from a subset of the August data, we next attempted to coherently add all the additional August data segments. We did this by adding data segments one at a time into the total Z_1^2 sum and then used the *IDL* function minimizer/maximizer *tnmin* to optimize the solution (Markwardt 2009). In each case Z_1^2 increased in a monotonic fashion, and the orbit parameters remained consistent. Phasing up all the August data in this way resulted in a peak value of $Z_1^2 = 196.1$. Recall that in the case of pure Poisson noise, the Z_1^2 statistic is distributed as χ^2 with 2 degrees of freedom, and a value this high has a chance probability (single trial) of 2.6×10^{-43} (13.8 σ). The pulsed signal after accounting for the orbital phase delays is

dramatically stronger than with no orbit correction, as expected. Figure 4 compares these two signals. The curves show Z_1^2 evaluated on a grid of ν_0 with orbit phase delays included (black), and without (red). We note that, as in Figure 2, the modulating "comb" of finely spaced sub-peaks results from the observing window function. Using the full August data set we find the best orbital solution has $P_{orb} = 2277.89 \pm 0.48$ s, $a_x \sin i/c = 0.00395 \pm 0.0003$ lt-sec, $\nu_0 = 163.65611058 \pm 2.7 \times 10^{-7}$ Hz, and $T_0 =$ MJD 57974.82835$\pm$0.0007 (TDB), where we quote nominal 3σ errors for a single parameter by finding the values for each parameter at which $\Delta Z_1^2 = 9$ (Markwardt et al. 2002).

We then carried out similar analyses on the October and November data segments, treated separately, and found consistent results. Finally, we combined data across all epochs, and found a peak $Z_1^2 = 355.4$. We again determined confidence regions using $\Delta Z_1^2 = 9$, and found the best solution has $P_{orb} = 2278.208 \pm 0.012$ s (37.97 min), $a_x \sin i/c = 0.00389 \pm 0.0002$ lt-sec, $\nu_0 = 163.656110496 \pm 9 \times 10^{-9}$ Hz, and $T_0 =$ MJD 57974.82795 $\pm$ 0.00028 (TDB). The timing solution is summarized in Table 1.

Next, we allowed the eccentricity, e, to be non-zero, but this did not result in a significant increase in Z_1^2, and we placed an upper limit on it of $e < 0.03$ (1σ, $\Delta Z_1^2 = 1$). Using our best orbit solution we phase-folded all the data, and fit the resulting pulse profile (0.3 - 3.2 keV) with a sinusoid, $A + B\sin(\phi - \phi_0)$. The fit is excellent, with a minimum $\chi^2 = 8.6$ (13 degrees of freedom), and the implied fractional pulsed amplitude is $B/A = 2.04 \pm 0.11\%$. Figure 5 shows the resulting pulse profile and fitted model. We did not detect any harmonic signals. We note that the pulsed amplitude measured with *NICER* is comfortably below the upper limits reached in the recent pulsation search with *XMM-Newton* reported by van den Eijnden et al. (2018), which likely explains why they did not detect the pulsations. We also computed pulse phase residuals using the best orbit solution. We show these in Figure 6, where we have added in the orbit-predicted phase delay in order to visually show the size of the delays. We did not find any statistically significant long-term trends in these residuals. Finally, we allowed for a constant pulsar spin frequency derivative, $\dot{\nu}$, in the timing model, and recomputed Z_1^2 on a grid of ν_0 and $\dot{\nu}$ values. We found no significant increase in Z_1^2, and we derived the following limits, $-6 \times 10^{-15} < \dot{\nu} < 4 \times 10^{-15}$ Hz s^{-1} (1σ).

4. DISCUSSION AND SUMMARY

Our analysis of observations of J1706 with *NICER* obtained in 2017 August, October and November confirms the discovery by SK17 that it is a 163.656 Hz AMXP, and allowed us to derive the orbital parameters of the system for the first time. The 37.97 min orbital period of J1706 is the shortest currently known for an AMXP, and our measurement confirms several previous indirect indications that the system is an ultracompact binary (Hernandez Santisteban et al. 2018; van den Eijnden et al. 2018). We measure a mass function, $f_x = (m_d \sin i)^3/(m_{ns} + m_d)^2 = ((a_x \sin i)^3 \omega_{orb}^2)/G = 9.12 \times 10^{-8} M_\odot$, which is also the smallest among stellar binaries. The mass function

Table 1. Timing Parameters for IGR J17062-6143

Parameter	Value
Right ascension, α (J2000)	256.5677°
Declination, δ (J2000)	−61.7113°
Barycentric pulse frequency, ν_0 (Hz)	163.656110049(9)
Pulsar frequency derivative, $\dot{\nu}$ (Hz s^{-1})	$-6 \times 10^{-15} < \dot{\nu} < 4 \times 10^{-15}$
Projected semi-major axis, $a_x \sin(i)/c$ (lt - s)	0.0039(2)
Binary orbital period, P_{orb} (s)	2278.208(12)
Time of mean longitude equal to zero, T_0	MJD 57974.82795(28) (TDB)
Orbital eccentricity, e	< 0.03
Pulsar mass function, f_x ($10^{-8} M_\odot$)	9.12(2)
Minimum donor mass, m_d ($M_\odot$)	0.005 - 0.007
Maximum Z_1^2 power	355.4

NOTE—Parameter uncertainties for ν_0, $a_x \sin(i)/c$, P_{orb} and T_0 are 3σ ($\Delta Z_1^2 = 9$) values, given in the last quoted digits. Limits for e, and $\dot{\nu}$ are 1σ. The minimum donor mass range is for neutron star masses of 1.2 and 2 $M_\odot$.

defines a lower limit to the mass of the donor star, m_d. For a neutron star mass in the range from $m_{ns} = 1.2 - 2M_\odot$ we find a minimum donor mass in the range from $0.005 - 0.007 M_\odot$. Given the orbital period and a plausible range of total system mass, the separation between the components is of order 300,000 km, and would fit within the Earth - Moon distance.

The reasonable assumption that the donor star fills its Roche lobe provides a constraint on the mean density of the donor. This can be expressed as a constraint on its radius in units of the component separation, a, that depends principally on the system's mass ratio, $q = m_d/m_{ns}$ (Eggleton 1983). We combine this constraint with that from the measured mass function to explore the implications for the nature of the donor star and the system's orbital inclination.

Our results are summarized in Figure 7 which shows constraints on the donor mass and radius. We plot the Roche lobe constraint for three different neutron star masses, 1.2 (green), 1.4 (black), and 1.8 $M_\odot$ (red). The closeness of the three curves is a visual demonstration of how insensitive this constraint is to the assumed neutron star mass. The different symbols along the curve mark inferred donor masses from the mass function constraint for different assumed orbital inclinations, i, and for two values of the neutron star mass at each inclination. For each pair of symbols the left- and right-most correspond to a neutron star mass of 1.2 and $1.8 M_\odot$, respectively. The left-most symbol for $i = 90°$ marks the minimum donor mass for a $1.2 M_\odot$ neutron star. First, we note that the constraints require hydrogen-deficient donors, as is expected

for systems with an orbital period less than about 80 min (Rappaport & Joss 1984; Bildsten 2002). For additional context we show mass - radius relations obtained from the literature for several donor types. The dashed curve is the mass - radius relation for low mass, cold, pure helium white dwarfs from Zapolsky & Salpeter (1969), as corrected by Rappaport & Joss (1984). Here we have plotted it using the fitting formula of Nelemans et al. (2001). The dotted curves denote a range of mass - radius values from the binary evolutionary calculations of Deloye et al. (2007) for the helium donors of AM CVn systems. The region between the upper and lower dotted curves gives an indication of the allowed range in mass and radius for donors at different evolutionary stages, and with different values of central degeneracy at the onset of mass transfer (see Deloye et al. 2007 for details). Lastly, the dash-dotted curves show mass - radius relations for carbon white dwarfs with central temperatures of 10^4 (lower) and 3×10^6 K (upper), from Deloye & Bildsten (2003). Thus, J1706 appears to be a somewhat more extreme example of the currently known ultracompact AMXPs (Krimm et al. 2007; Patruno & Watts 2012).

For a random distribution of inclination angles the chance probability to observe a system with an inclination less than or equal to i is $1-\cos(i)$. The probability to observe an inclination angle less than or equal to $\approx 18.2°$ is 5%. From this, and assuming a $1.8M_\odot$ neutron star mass, we deduce a 95% confidence upper limit to the donor mass of $0.0216M_\odot$, with a corresponding radius of $0.05R_\odot$, substantially less than that of any hydrogen-rich brown dwarfs (Chabrier et al. 2000). We use this upper limit on the donor radius to place an upper limit on the inclination of $\approx 84°$, since no eclipses are seen in the light curve.

Additional insight is provided by estimates of the long term mass accretion rate, $\dot{M}$, and the realization that the mass transfer in such systems is driven by angular momentum loss due to gravitational radiation (Rappaport & Joss 1984; Bildsten & Chakrabarty 2001). Interestingly, for J1706 we have $\dot{M}$ estimates from both persistent X-ray flux measurements and modeling of its thermonuclear X-ray bursts that are in substantial agreement (Keek et al. 2017), and suggest $\dot{M} \approx 2.5\times10^{-11}\ M_\odot\ \mathrm{yr}^{-1}$. This value for J1706 is also in general agreement with the calculations of $\dot{M}$ versus P_{orb} reported by Deloye et al. (2007, see their Figure 15). Based on this, and the reasonable assumption that the donor responds to mass loss like a degenerate star (Bildsten & Chakrabarty 2001), we can estimate the donor mass as $m_d = 0.0175(m_{ns}/1.4M_\odot)^{-1/3}\ M_\odot$. Using this result we additionally show in Figure 7 (with blue "+" symbols) the donor masses and corresponding radii for neutron star masses of 1.4 and 2 $M_\odot$, where the higher donor mass estimate corresponds to the lower mass neutron star (1.4 $M_\odot$). These mass estimates further imply constraints on the binary inclination angle of $19° < i < 27.5°$, where the lower and upper bounds correspond to neutron star masses of 1.4 and 2 $M_\odot$, respectively.

The constraints summarized in Figure 7 suggest that J1706 is observed at relatively low inclination, and the donor mass - radius constraints appear to be consistent with

the helium donors of AM CVn systems explored by (Deloye et al. 2007) (the dotted curves in Figure 7). We note that these authors also provide estimates of the expected orbital period evolution, $\dot{P}_{orb}$, for these systems. Given the observed orbital period of J1706, the predicted values are in the range $\dot{P}_{orb} \approx 1 - 3 \times 10^{-6}$ s yr^{-1}, which can be probed with additional *NICER* timing observations.

Clues to the donor composition in a neutron star X-ray binary can in principle be provided by the properties of its thermonuclear flashes. The energetic, long duration burst events seen to date would appear to be consistent with deep ignition of a helium-rich layer (Keek et al. 2017). As noted previously, under certain conditions the stable burning of accreted hydrogen into helium can result in helium-powered thermonuclear flashes (Fujimoto et al. 1981; Galloway & Cumming 2006). Our measurements confirm the previous indications for a hydrogen-deficient donor in J1706 (Hernandez Santisteban et al. 2018; van den Eijnden et al. 2018), and definitively rule out this option, since the accreted fuel cannot contain a significant fraction of hydrogen.

While a helium donor in J1706 appears quite plausible given the measurements presented here, as well as its bursting properties, prior X-ray spectroscopy results have suggested J1706 may have an oxygen-rich circumbinary environment, perhaps associated with an outflow (van den Eijnden et al. 2018). In addition, spectral modeling of the Fe Kα reflection feature appears to favor a higher inclination than suggested by our constraint derived from the assumption of gravitational radiation driven mass loss (Degenaar et al. 2017; van den Eijnden et al. 2018; Keek et al. 2017). Based on these indications, van den Eijnden et al. (2018) favor a CO or O-Ne-Mg white dwarf donor. Given the constraints on the donor summarized in Figure 7 this remains a viable option, particularly in the case of non-conservative mass transfer, as would occur in the presence of an outflow. However, such a conclusion would also open up additional questions, such as the nature of the fuel for the observed X-ray bursts, which is presumably helium (Keek et al. 2017), though we note that Hernandez Santisteban et al. (2018) did not detect helium in their optical spectra of J1706. Further to this final point, the bursting low mass X-ray binary 4U 0614+091 is another source with apparently helium-powered X-ray bursts (Kuulkers et al. 2010), but whose optical spectra are suggestive of a CO donor with little to no helium (Werner et al. 2006; Nelemans et al. 2004). Additional observations will likely be needed to definitively pin down the nature of the donor in J1706.

While most AMXPs are transient systems, J1706 is distinctive in that it has been in outburst now for about a decade. This provides an exciting opportunity to study the long-term spin and orbital evolution with additional *NICER* observations. Moreover, we now have detections of pulsations from J1706 at two widely spaced epochs, in 2008 May with *RXTE*, and the present 2017 August, October and November observations with *NICER*. Interestingly, the source shows some indications of a significant change in pulsed amplitude in that time-frame. The estimated source pulsed amplitude

measured by SK17 with *RXTE* was $9.4 \pm 1.1\%$ $(2-12$ keV), whereas we find $2.04 \pm 0.11\%$ $(0.3-3.2$ keV) with *NICER*. We note that given the current uncertainties associated with modeling the *NICER* background, combined with the fact that the source count rate is dropping steadily above ≈ 5 keV, it is presently challenging to accurately determine the pulsed amplitude above this energy. Nevertheless, with the present data we can measure the pulsed amplitude in the $2-5$ keV band with reasonable precision, and we find a value of $3.2 \pm 0.3\%$. Based on this we think it likely that the smaller amplitude measured by *NICER* is a real effect and likely represents some secular change within the system, perhaps associated with the effect of accretion on the magnetic field, as, for example, suggested by Patruno (2012). More definitive conclusions in this regard should become feasible as the *NICER* background calibration improves. We will pursue this, as well as searches for energy dependent phase lags and a detailed spectroscopic study in subsequent work.

This work was supported by NASA through the *NICER* mission and the Astrophysics Explorers Program. This research also made use of data and/or software provided by the High Energy Astrophysics Science Archive Research Center (HEASARC), which is a service of the Astrophysics Science Division at NASA/GSFC and the High Energy Astrophysics Division of the Smithsonian Astrophysical Observatory. SG acknowledges the support of the Centre National dEtudes Spatiales (CNES). We thank the anonymous referee for a helpful report.

Facility: NICER, ADS, HEASARC

Software: HEAsoft (v6.22; Arnaud 1996), mpfit (Markwardt 2009)

REFERENCES

Bildsten, L. 2002, ApJL, 577, L27, doi: 10.1086/344085

Bildsten, L., & Chakrabarty, D. 2001, ApJ, 557, 292, doi: 10.1086/321633

Blandford, R., & Teukolsky, S. A. 1976, ApJ, 205, 580, doi: 10.1086/154315

Bradt, H. V., Rothschild, R. E., & Swank, J. H. 1993, A&AS, 97, 355

Buccheri, R., Bennett, K., Bignami, G. F., et al. 1983, A&A, 128, 245

Chabrier, G., Baraffe, I., Allard, F., & Hauschildt, P. 2000, ApJ, 542, 464, doi: 10.1086/309513

Churazov, E., Sunyaev, R., Revnivtsev, M., et al. 2007, A&A, 467, 529, doi: 10.1051/0004-6361:20066230

Degenaar, N., Miller, J. M., Wijnands, R., Altamirano, D., & Fabian, A. C. 2013, ApJL, 767, L37, doi: 10.1088/2041-8205/767/2/L37

Degenaar, N., Pinto, C., Miller, J. M., et al. 2017, MNRAS, 464, 398, doi: 10.1093/mnras/stw2355

Deloye, C. J., & Bildsten, L. 2003, ApJ, 598, 1217, doi: 10.1086/379063

Deloye, C. J., Taam, R. E., Winisdoerffer, C., & Chabrier, G. 2007, MNRAS, 381, 525, doi: 10.1111/j.1365-2966.2007.12262.x

Eggleton, P. P. 1983, ApJ, 268, 368, doi: 10.1086/160960

Fujimoto, M. Y., Hanawa, T., & Miyaji, S. 1981, ApJ, 247, 267, doi: 10.1086/159034

Galloway, D. K., & Cumming, A. 2006, ApJ, 652, 559, doi: 10.1086/507598

Gendreau, K. C., Arzoumanian, Z., & Okajima, T. 2012, in Proc. SPIE, Vol. 8443, Space Telescopes and Instrumentation 2012: Ultraviolet to Gamma Ray, 844313

Hernandez Santisteban, J. V., Cuneo, V., Degenaar, N., et al. 2018, ArXiv e-prints. https://arxiv.org/abs/1801.03006

Keek, L., Iwakiri, W., Serino, M., et al. 2017, ApJ, 836, 111, doi: 10.3847/1538-4357/836/1/111

Krimm, H. A., Markwardt, C. B., Deloye, C. J., et al. 2007, ApJL, 668, L147, doi: 10.1086/522959

Kuulkers, E., in't Zand, J. J. M., Atteia, J.-L., et al. 2010, A&A, 514, A65, doi: 10.1051/0004-6361/200913210

Leahy, D. A., Darbro, W., Elsner, R. F., et al. 1983, ApJ, 266, 160, doi: 10.1086/160766

Markwardt, C. B. 2009, in Astronomical Society of the Pacific Conference Series, Vol. 411, Astronomical Data Analysis Software and Systems XVIII, ed. D. A. Bohlender, D. Durand, & P. Dowler, 251

Markwardt, C. B., Swank, J. H., Strohmayer, T. E., in 't Zand, J. J. M., & Marshall, F. E. 2002, ApJL, 575, L21, doi: 10.1086/342612

Negoro, H., Serino, M., Sasaki, R., et al. 2015, The Astronomer's Telegram, 8241

Nelemans, G., Jonker, P. G., Marsh, T. R., & van der Klis, M. 2004, MNRAS, 348, L7, doi: 10.1111/j.1365-2966.2004.07486.x

Nelemans, G., Portegies Zwart, S. F., Verbunt, F., & Yungelson, L. R. 2001, A&A, 368, 939, doi: 10.1051/0004-6361:20010049

Patruno, A. 2012, ApJL, 753, L12, doi: 10.1088/2041-8205/753/1/L12

Patruno, A., & Watts, A. L. 2012, ArXiv e-prints. https://arxiv.org/abs/1206.2727

Ransom, S. M., Cordes, J. M., & Eikenberry, S. S. 2003, ApJ, 589, 911, doi: 10.1086/374806

Rappaport, S., & Joss, P. C. 1984, ApJ, 283, 232, doi: 10.1086/162298

Remillard, R. A., & Levine, A. M. 2008, The Astronomer's Telegram, 1853

Ricci, C., Beckmann, V., Carmona, A., & Weidenspointner, G. 2008, The Astronomer's Telegram, 1840

Strohmayer, T., & Keek, L. 2017, ApJL, 836, L23, doi: 10.3847/2041-8213/aa5e51

Strohmayer, T. E., & Markwardt, C. B. 2002, ApJ, 577, 337, doi: 10.1086/342152

van den Eijnden, J., Degenaar, N., Pinto, C., et al. 2018, MNRAS, 475, 2027, doi: 10.1093/mnras/stx3224

Werner, K., Nagel, T., Rauch, T., Hammer, N. J., & Dreizler, S. 2006, A&A, 450, 725, doi: 10.1051/0004-6361:20053768

Zapolsky, H. S., & Salpeter, E. E. 1969, ApJ, 158, 809, doi: 10.1086/150240

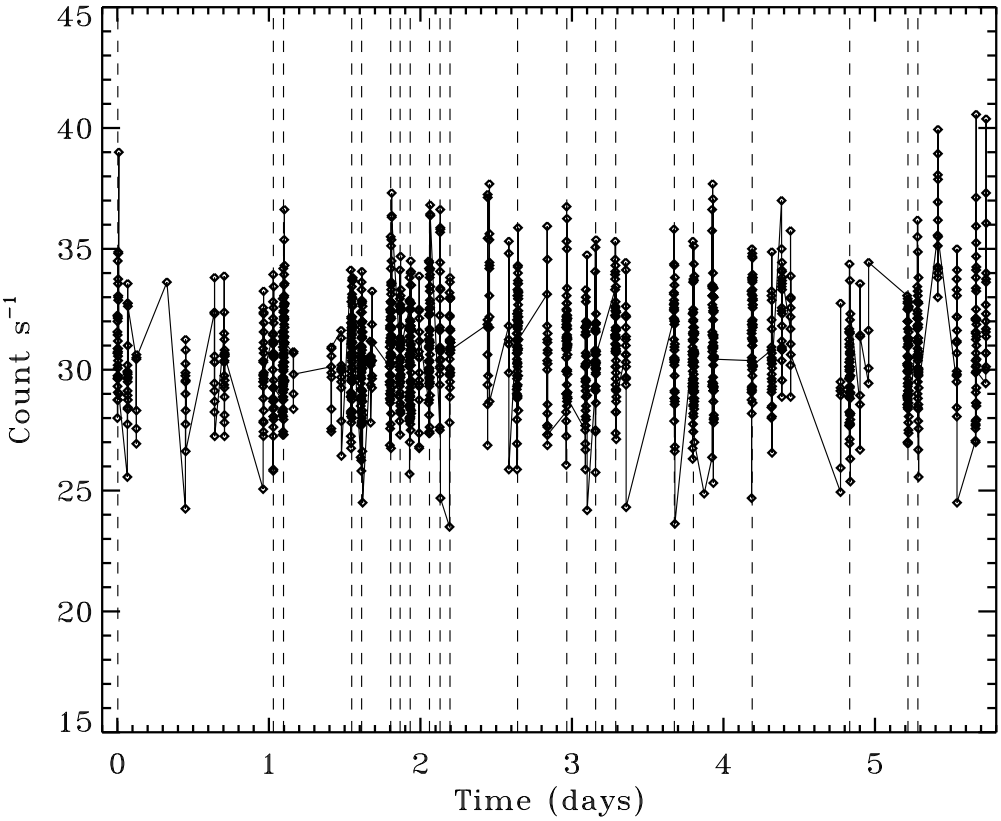

Figure 1. Light curve of J1706 from *NICER* observations obtained in 2017 August. Data are the summed counting rates in 16 s bins in the 0.3 - 5 keV band. The vertical dashed lines mark the centers of 21 good time intervals used to compute average power spectra (see §2). Time zero is MJD 57974.8334963496 (TDB).

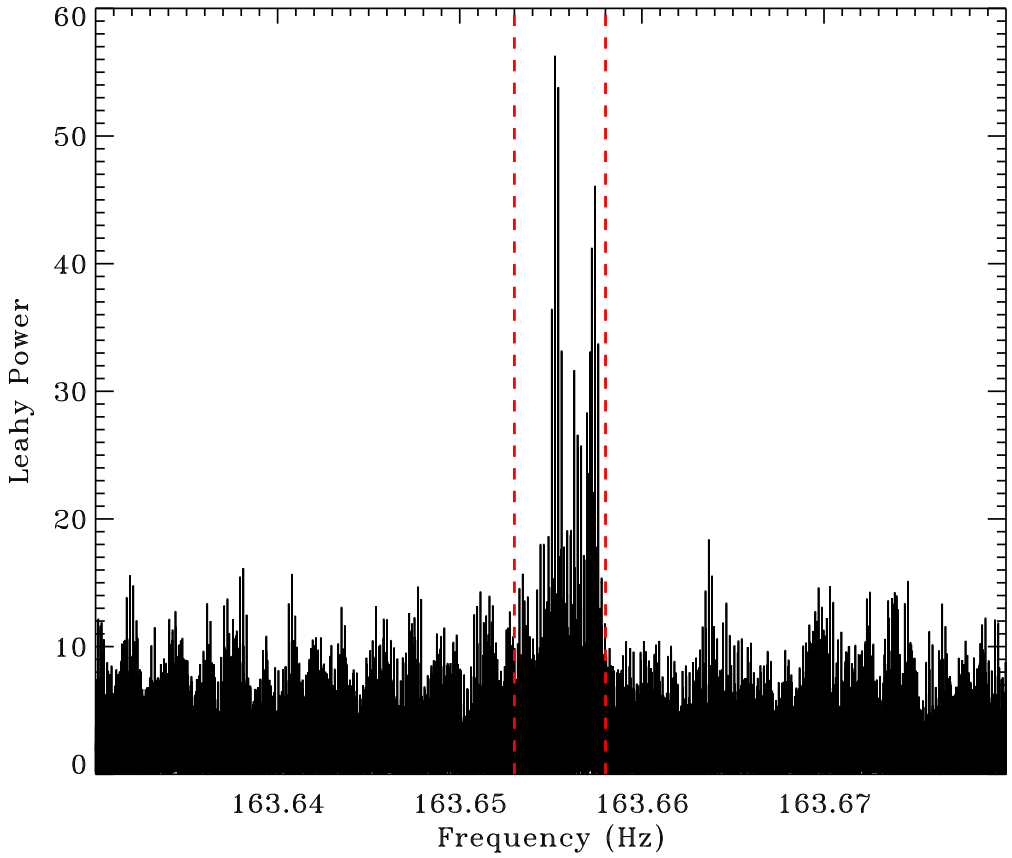

Figure 2. Power spectrum of J1706 from *NICER* observations obtained in 2017 August, in the vicinity of the pulse frequency detected with *RXTE* by SK17. The spectrum was computed from a light curve spanning 500 ksec and sampled at 4096 Hz, and includes events in the 0.3 - 3.2 keV band. The 163.656 Hz pulsar peak is clearly evident. The vertical red lines indicate the approximate range of pulse frequency detected in the *RXTE* observations. See §2 for a detailed discussion of the pulsation search.

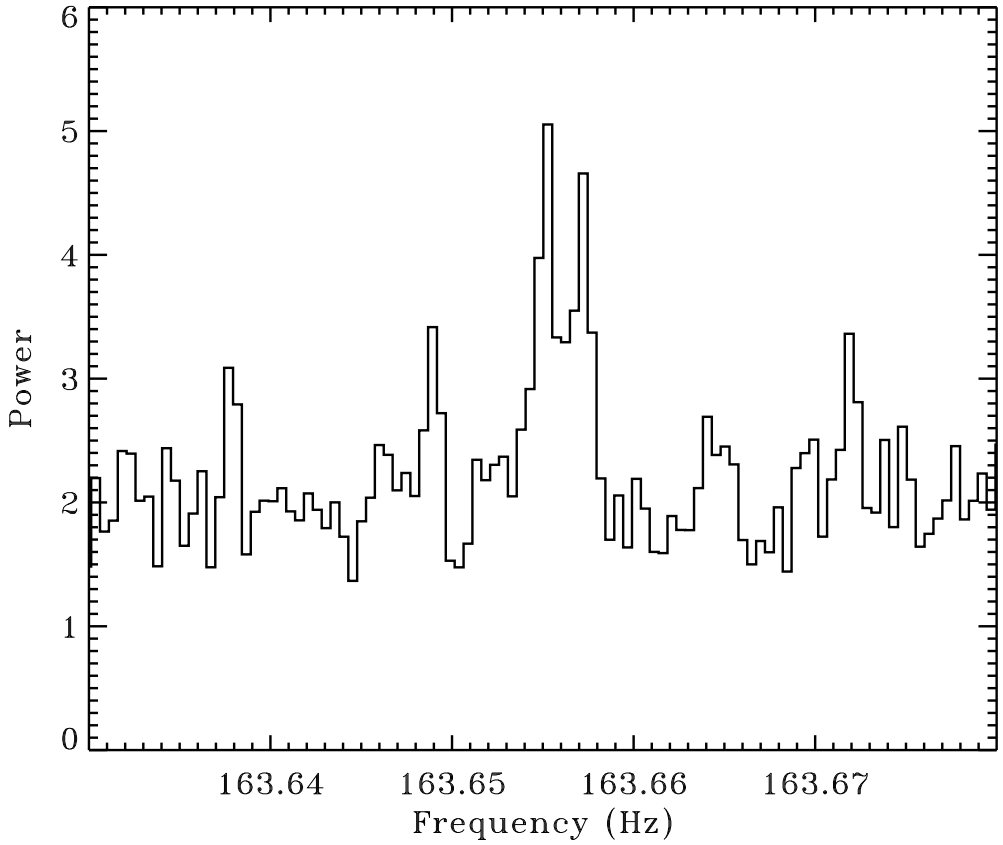

Figure 3. Average power spectrum of J1706 from *NICER* observations obtained in 2017 August, in the vicinity of the 163.656 Hz pulsar frequency, computed from 21 on-source dwells with exposures ranging from 1294 s (longest) to 545 s (shortest). The pulsar signal is comprised of two dominant side-bands. See §2 for a detailed discussion of the pulsation search.

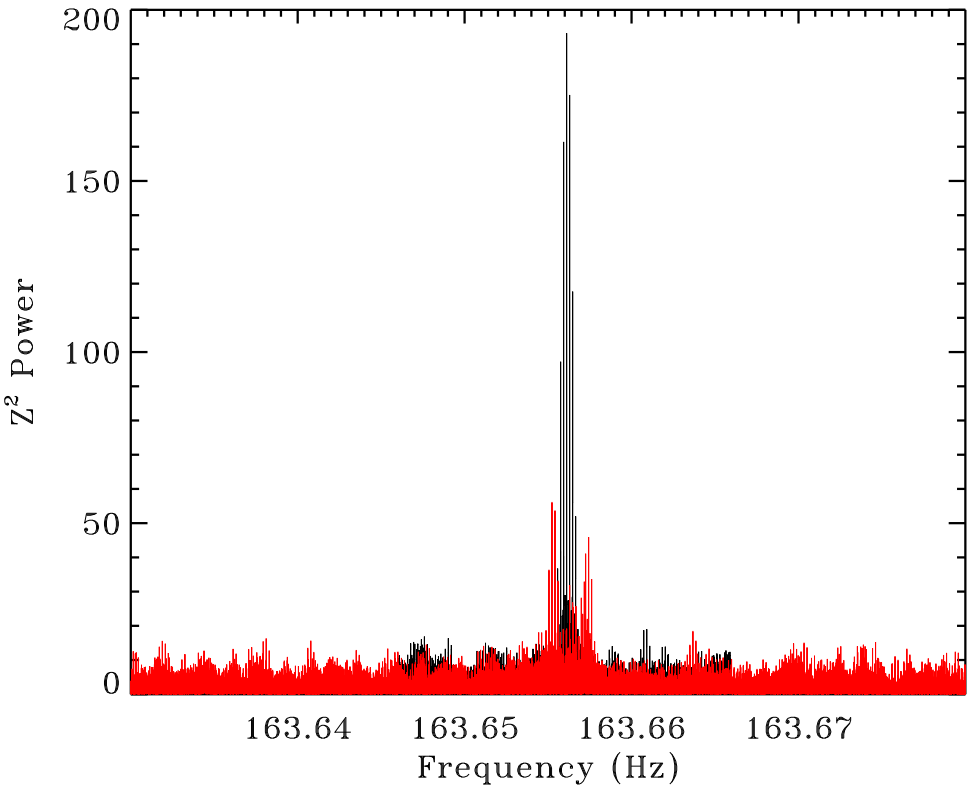

Figure 4. Comparison of the Z_1^2 signals for the August *NICER* data with and without the orbital phase delays. The curves show Z_1^2 evaluated on a grid of pulsar frequency, ν_0, with orbit phase delays included (black), and without (red). The orbit solution recovers a single, coherent peak with $Z_1^2 = 196.1$, modulated by the window function imposed by visibility from the *ISS* orbit. See §3 for a detailed discussion of the orbit search.

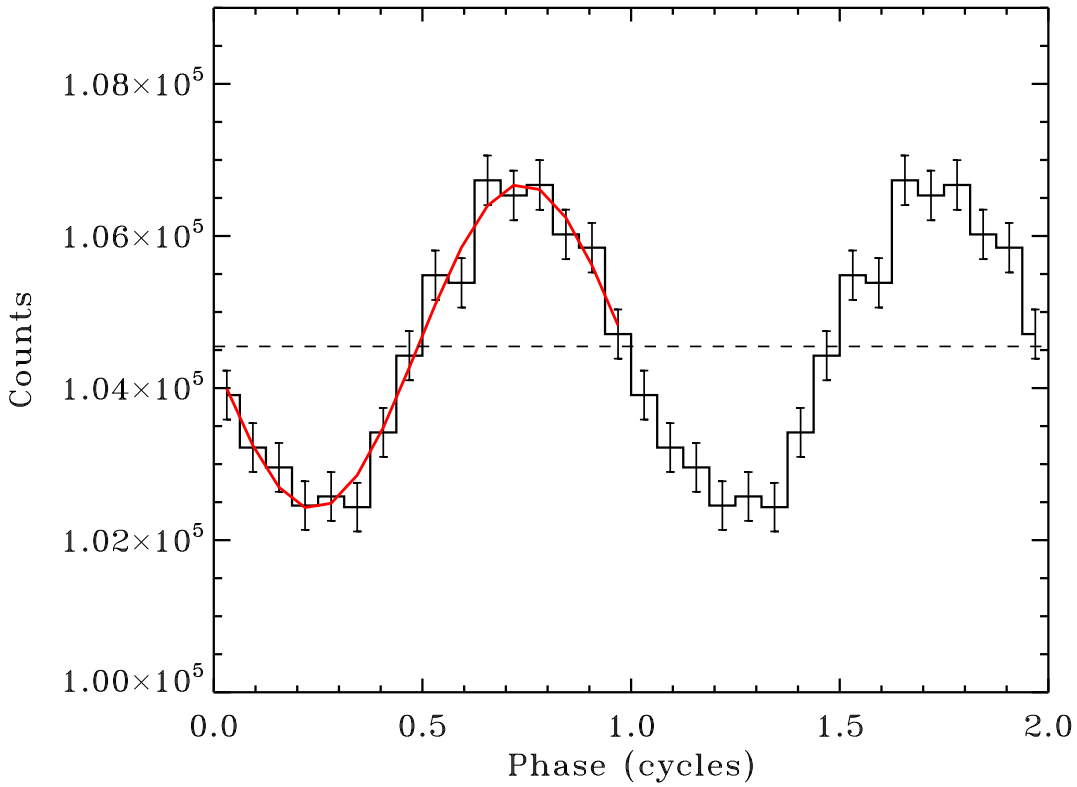

Figure 5. Pulse profile obtained after phase folding the August, October and November *NICER* exposures of J1706 with the best-determined orbital solution. The profile includes events in the 0.3 - 3.2 keV range, and we used 16 phase bins. The best fitting sinusoid, $A + B\sin(\phi)$, is also plotted (red). The fit has $\chi^2 = 8.6$ with 13 degrees of freedom. The pulsed amplitude is $B/A = 2.04 \pm 0.11\%$.

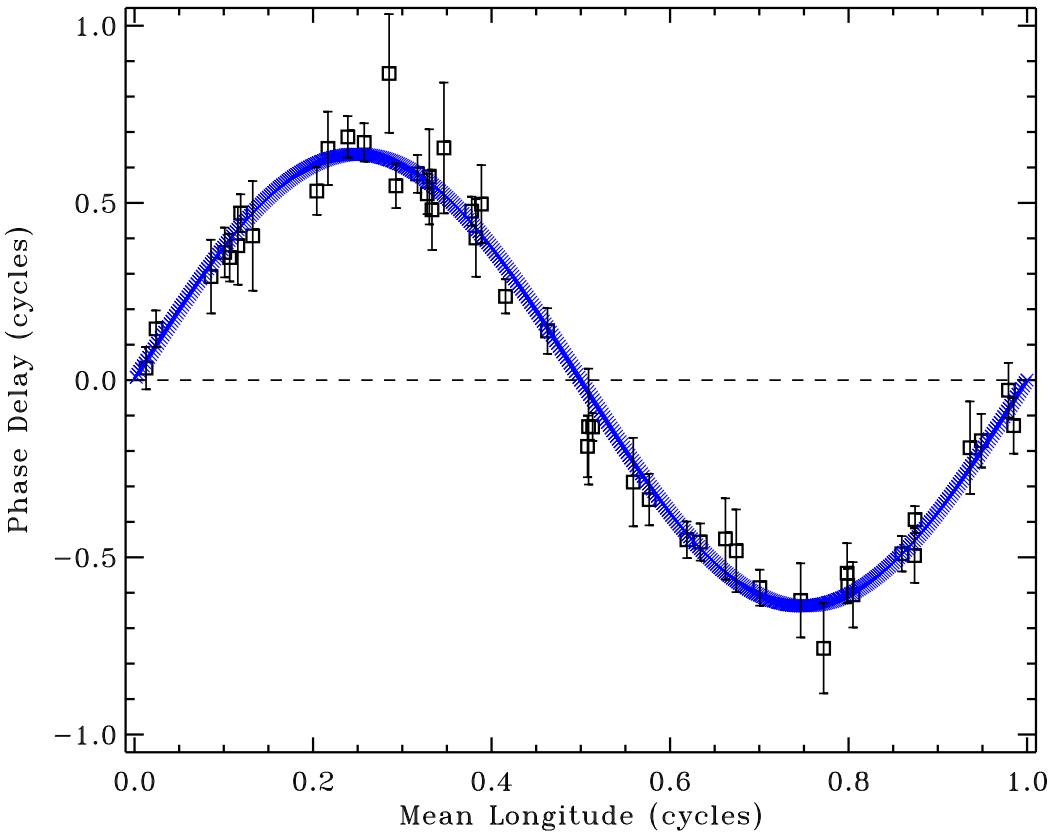

Figure 6. Pulse phase residuals from *NICER* observations of J1706 as a function of mean pulsar longitude computed using the best orbit solution. The residual is plotted in units of pulsar phase (cycles), and the orbit-predicted phase delay is added to the residuals to show the orbital variations.

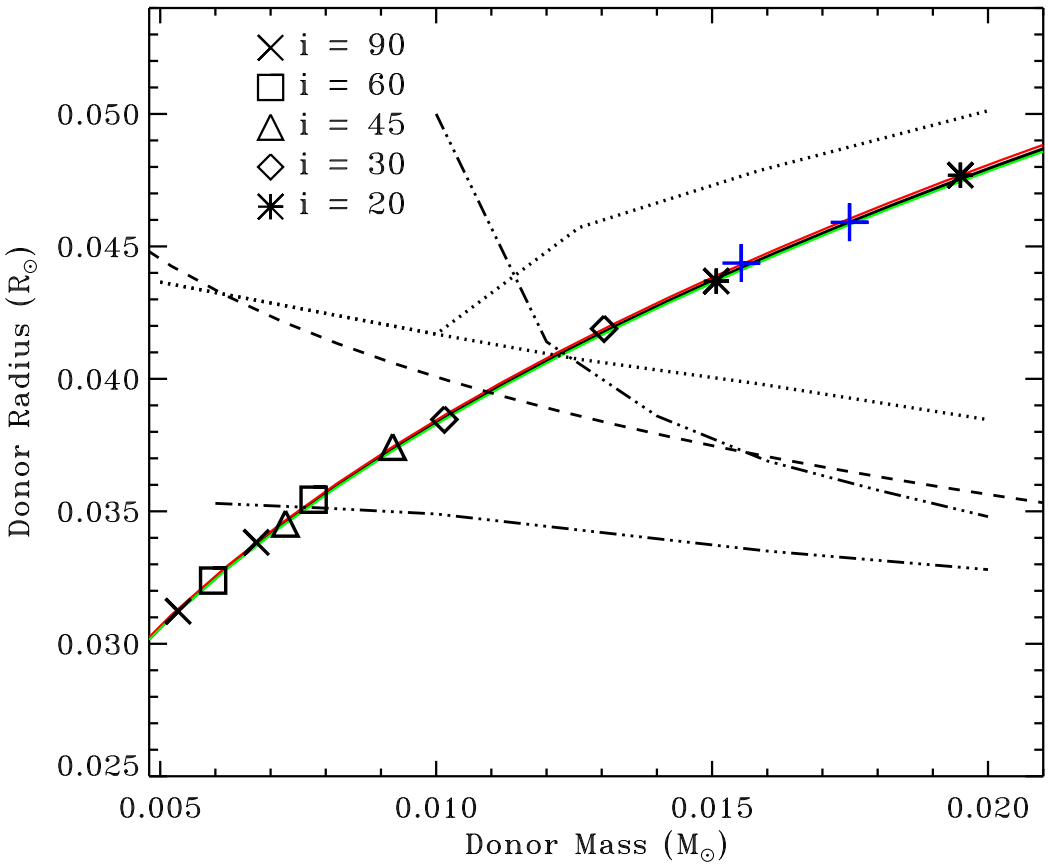

Figure 7. Constraints on the donor in J1706. The Roche lobe constraint is plotted for three different neutron star masses, 1.2 (green), 1.4 (black), and 1.8 $M_\odot$ (red). The different symbols along the curves denote donor masses from the mass function constraint for different assumed inclinations, i, and for two values of the neutron star mass at each inclination. For each pair of symbols the left- and right-most correspond to neutron stars of 1.2 and 1.8$M_\odot$, respectively. Also shown are mass - radius relations obtained from the literature for several donor types. The dashed curve is the fitting formula from Nelemans et al. (2001) that approximates the mass - radius relation for low mass, cold, pure helium white dwarfs (Zapolsky & Salpeter 1969). The dotted curves denote a range of mass - radius values from the binary evolutionary calculations of Deloye et al. (2007) for the helium donors of AM CVn systems. The dash-dotted curves show mass - radius relations for carbon white dwarfs with central temperatures of 10^4 (lower) and 3×10^6 K (upper), from Deloye & Bildsten (2003). Lastly, the blue "+" symbols mark the masses and radii that would produce a long-term $\dot{M} = 2.5 \times 10^{-11} M_\odot$ yr^{-1} via gravitational radiation for neutron stars of 1.4 (higher value) and 2 $M_\odot$ (lower value, see §4 for further discussion).